Growth and orientation relationships of Ni and Cu films annealed on slightly miscut (1-102) r-sapphire substrates

Dominique Chatain, Blandine Courtois, Igor Ozerov, Nathalie Bozzolo, Madeleine Kelly, Gregory S Rohrer, Paul Wynblatt

Growth and orientation relationships of Ni and Cu films annealed on slightly miscut (1 $\bar{1}$ 0 2) r-sapphire substrates

Dominique Chatain[a,*], Blandine Courtois[a], Igor Ozerov[a], Nathalie Bozzolo[b], Madeleine Kelly[c], Gregory S. Rohrer[c], Paul Wynblatt[c]

[a] Aix-Marseille Univ, CNRS, CINAM, 13009 Marseille, France
[b] MINES ParisTech, PSL – Research University, CEMEF, CNRS UMR 7635, 06904 Sophia Antipolis Cedex, France
[c] Department of Materials Science and Engineering, Carnegie Mellon University, Pittsburgh, PA 15213, USA

ARTICLE INFO

Communicated by Silvere Akamatsu

Keywords:
A3. Orientation relationship
A3. Thin film
A1. Grain growth
B1. EBSD
A3. Metal-sapphire interfaces

ABSTRACT

Nano-crystalline Ni and Cu films deposited on the r-plane of sapphire (α-Al_2O_3) develop a ⟨1 1 1⟩ fiber-texture upon annealing, in which grains grow up to 300 to 500 times larger than the film thickness. Most of the largest grains, which have grown at the expense of others, display one of four preferred orientation relationships (ORs) to the substrate. The four preferred ORs are OR1r = Me(1 1 1)[1 $\bar{1}$ 0]//α-Al_2O_3(1 $\bar{1}$ 0 2)[1 1 $\bar{2}$ 0], OR2r = Me(1 1 1)[1 $\bar{1}$ 0]//α-Al_2O_3(1 $\bar{1}$ 0 2)[$\bar{1}$ 1 0 1] (Me = Ni or Cu), and their twins, which are rotated 60° about the ⟨1 1 1⟩ axis perpendicular to the substrate. For these ORs, one of the densest ⟨1 1 0⟩ atomic rows that lies within the Me {1 1 1} interfacial plane, aligns with the direction of the step edges that form at the intersection of the r-plane with one of its neighboring facets on the equilibrium shape of sapphire (i.e. the c-(0 0 0 1), p-{1 1 $\bar{2}$ 3} or s{1 0 $\bar{1}$ 1}-planes). One of the ORs is most preferred when the steps at the interface are such that a {1 0 0}-type ledge of the Me {1 1 1} interfacial plane faces the ledge of the sapphire step. This observation provides a useful insight into the origin of the preferred ORs, and confirms the important role of surface steps in texture development. The evolution of Ni films of different thicknesses, ranging from 100 to 560 nm, was analyzed. Grain boundary grooving inhibits grain boundary motion and favors hole formation and dewetting in the thinnest films (100 nm). The crystals left behind after dewetting display ORs which may differ from the preferred ones. Large grains with the preferred ORs can grow at the expense of others when the film thickness is greater than 300 nm.

1. Introduction

Basic studies of the heteroepitaxy of metallic films on single-crystalline oxide substrates are aimed at understanding interfacial atomic structure and bonding, in order to predict the properties of the technologically important devices that contain them. For this purpose, interfaces have been investigated in model systems such as face-centered cubic (fcc) metallic films or particles grown on sapphire (α-Al_2O_3) substrates. However, for the most part, these studies have been limited to oxide substrates oriented along high symmetry crystallographic planes, such as the (0 0 0 1) c-plane of sapphire.

Polycrystalline fcc metallic films tend to develop a ⟨1 1 1⟩-fiber texture when annealed on substrates which do not match their lattice parameter. All possible orientations of the ⟨1 1 1⟩-fiber are not equally probable when the substrate is a single-crystal. Rather, the metallic grains may develop a number of orientation relationships (ORs) with the substrate. The same ORs on the c-plane of sapphire have been found for Al, Cu, Ni and Pt, in the form either of polycrystalline films annealed after deposition, or of crystallites produced by solid-state dewetting of the films [1–15]. The large atomic lattice mismatch between sapphire and these metals rules out the possibility that a coherent interface will develop in order to minimize the interfacial strain energy. The preferred ORs adopted by these metals correspond to the alignment of one of the close packed ⟨1 1 0⟩ directions that lie in their interfacial {1 1 1} planes, with particular directions of the substrate surface, and display very large interfacial unit cells (see for example [11]). It has also been observed that the preferred OR of large grains of Al [1,3] and Cu crystals [10] on the c-plane of sapphire depends on the annealing temperature.

Recent work on heteroepitaxy, which has made use of polycrystalline substrates, so as to cover the whole range of possible substrate orientations, has allowed a better picture of the mechanisms that

* Corresponding author.
E-mail address: chatain@cinam.univ-mrs.fr (D. Chatain).

https://doi.org/10.1016/j.jcrysgro.2018.11.024

control thin film epitaxy to emerge, and has shed light on the important role of atomic steps at the interface. Such studies have been performed on two types of systems, metal on metal (Ag on Ni [16,17]), and oxide on oxide (tin oxide on columbite [18]), by the technique of electron backscatter diffraction (EBSD) in a scanning electron microscope (SEM). A similar approach applied to metal-metal oxide interfaces would be useful to improve understanding of heteroepitaxy in these systems. Here, we take a first step in that direction by presenting a detailed study of the behavior of metal films on a sapphire substrate with an orientation other than the closest packed and high symmetry (0 0 0 1) c-plane.

This paper addresses the ORs and microstructures that develop during annealing of nano-crystalline Ni films deposited on the (1 $\bar{1}$ 0 2) r-plane of sapphire, and analyzes the conditions which lead to the growth of large grains. The r-plane has a high atomic density and is a stable facet on the equilibrium crystal shape of sapphire [19,20], but has a lower crystallographic symmetry than the c-plane. The analysis of our experimental results includes an investigation of the substrate steps, the presence of which are unavoidable for substrates that exceed a few microns in size. Grain growth of another fcc metallic film (Cu) on the same substrate produces the same set of ORs as Ni, although the relative fractions of these ORs are different. The results show that the preferred ORs are induced in the film by the directions of substrate steps that result from the miscut of the sapphire crystal during wafer production.

2. R-sapphire substrate crystallographic structure

It is convenient to employ a terrace-ledge-kink (TLK) description of the surfaces that constitute both sides of the substrate/film interface. These surfaces consist of terraces and steps, and the surface steps may further be decomposed into ledges and kinks [21]. The orientations of each of the three TLK components of a surface will be described in terms of the Miller indices of their surface planes. In some cases it may be convenient to describe the edges at the intersection between the terraces and ledges, in which case these will be described by their direction Miller indices.

Since a substrate surface is never perfectly flat, it will consist of terraces separated by steps, and these steps might determine the resulting OR of the film, as has been demonstrated in the case of Ag films on Ni substrates of 200 different orientations [16,17]. For the sapphire surface, the terrace, ledge and kink orientations have been taken to be the stable facets present on the sapphire equilibrium crystal shape (ECS), as reported in several papers [19,20,22,23]. For the purest crystals, two different investigations [19,20] agree on the surface planes which are stable at temperatures above 1873 K in air; they are the c-, r-, p-, s- and a-planes. These planes are identified in Fig. 1a, which is a sketch of the fully facetted ECS of sapphire, calculated using the Wulffmaker software [24], with the relative facet surface energies reported in Ref. [19] at 2073 K. It is easy to identify four kinds of edges that run between the r-plane and the intersecting adjacent facets (or ledges), namely the c-, s-, p- and a-planes. Fig. 1b is the corresponding stereogram that displays the poles of these planes and the zone of the (1 1 $\bar{2}$ 0) pole (dashed vertical line) and of the (1 $\bar{1}$ 0 5) pole (horizontal line). Table 1 gives the indices of several planes, their corresponding perpendicular directions, and the direction of the edge shared by two connected planes at the periphery of the r-plane and of the c-plane. Some of these planes and directions will be used below to interpret issues related to the discussion of orientation relationships. Finally, the ionic structure of the r-plane is shown schematically in Fig. 1c.

Substrates of about 8 × 8 mm were cut out of single-side epipolished r-sapphire wafers,[1] 5.08 cm in diameter, 0.43 mm thick, with a maximum miscut angle from the r-plane of 0.1°. Profilometer traces taken along different diameters of the wafer showed a maximum curvature of 0.002°. The impurity content of the wafers (in wt ppm) was: Na < 4, Si < 3, Fe < 4, Mg < 1, Ni < 3, Ti < 1, Cu < 3, Mn < 3, Ca < 5.

3. Experiments with Ni films

Sample preparation prior to annealing has been performed in a clean room in order to prevent possible contamination of surfaces by air-suspended dust particles.

After scribing with a diamond tip and cleaving, substrates were ultrasonically cleaned for 5 min in acetone, another 5 min in isopropanol, rinsed in de-ionized water and dried under nitrogen flow. This aids in removing the sapphire dust produced by cutting the wafer.[2] Finally, the substrates were exposed to an oxygen plasma at 473 K for 10 min in a barrel reactor (Nanoplas, France) in order to burn off organic contaminants.

Nano-crystalline nickel thin films were deposited at room temperature on the sapphire substrates, at a rate of 0.7 nm/s under a vacuum of 5×10^{-4} Pa, from melted 99.995% pure nickel, heated in an alumina coated molybdenum crucible. The film thickness, which is constant on a given substrate, was monitored with a quartz microbalance during deposition, and measured by a contact profilometer afterwards. This thickness was varied from 100 nm to 560 nm. As will be shown later, in Fig. 3a, the nickel grain size at the surface of the film ranged from 20 to 30 nm. The microstructure of a 500 nm thick as-deposited film was investigated by X-ray diffraction. A θ–2θ out-of-plane scan showed all nickel peaks, except of the (2 0 0) peak, due to its overlap with the substrate peak. Thus, the as-deposited film did not have a strong texture or a preferred orientation relationship with the substrate.

The samples were heat treated at different temperatures ranging from 773 K (0.45 T_mNi, where T_mNi is the melting point of Ni, in K) to 1423 K (0.83 T_mNi), in one atmosphere of a 60% Ar + 40% H_2 gas mixture flowing at 10 cc/min, in an alumina tube fitted into a tube furnace. The heating rate to the annealing temperature was 25 K/min. Cooling from the annealing temperature occurred at the rate imposed by switching the furnace power off (it took about 2 h for the temperature to drop to about 723 K, where Ni diffusion becomes very slow [26]).

It is worth mentioning that the sapphire planes present on the sapphire ECS in air may be different from the ones that develop at low oxygen partial pressure, $P(O_2)$, when the sapphire is in contact with nickel (or copper) under a reducing atmosphere containing hydrogen. In what follows, we will see that the edges of the steps of the sapphire substrate remain the ones which are present at the sapphire substrate surface, prepared in air.

4. Results

4.1. Morphology and steps of the r-sapphire substrate used for the Ni films

The surfaces of two sapphire substrates, cut from the same wafer, were investigated by atomic force microscopy (AFM) in the tapping-mode. Both substrates were mounted in the AFM such that the flat edge on the wafer (45° counter-clockwise from the projection of the c-plane) from which they were cut, was positioned (within a few degrees) parallel to the left vertical side of the AFM images. Since the maximum surface curvature of the wafer was extremely low (0.002°), the miscut angle determines the surface morphology. Fig. 2a shows an AFM image

[1] Provided by CrysTec GmbH, Berlin, Germany.

[2] During sample annealing, sapphire dust particles act as centers of nucleation for holes at the interface between the nickel film and the sapphire substrate, and produce accelerated dewetting.

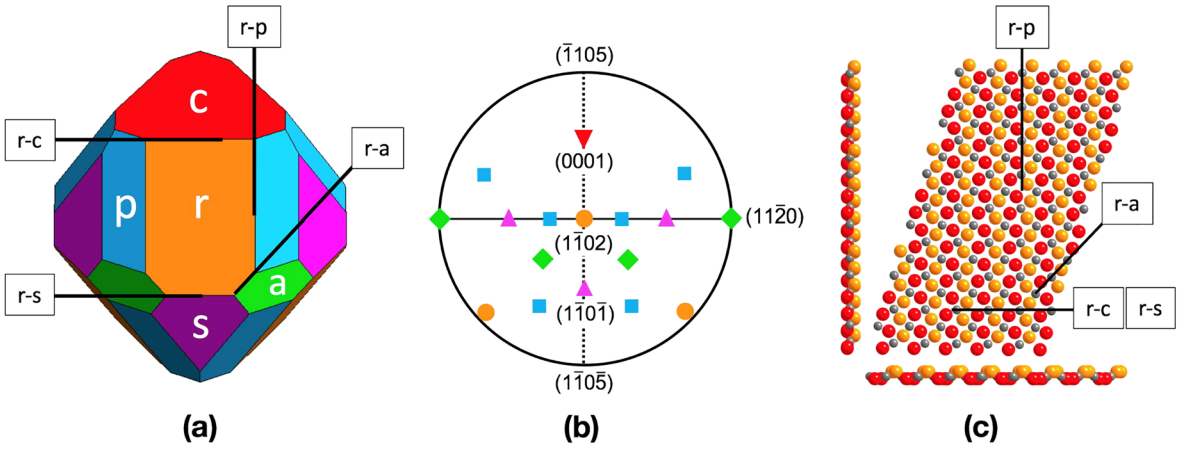

Fig. 1. (a) Fully facetted ECS of sapphire viewed along the direction perpendicular to the r-plane (orange), and showing the c-plane (red), the p-planes (blue), the s-planes (purple) and the a-planes (green); the 3 directions along which the r-plane intersects its 4 neighboring planes (c or s, p and a) are marked. When the r-plane is miscut towards either c or s, the step edges run along the [1 1 $\bar{2}$ 0] direction; a miscut towards the p-facet defines step edges running along the [1 $\bar{1}$ 0 1] direction; a miscut towards the a-facet defines step edges running along an almost [1 $\bar{1}$ 0 5] direction (see Table 1); (b) Corresponding sapphire stereogram, where the color code for the poles is the same as for the planes of the ECS plotted in (a); it is centered on a (1 $\bar{1}$ 0 2) pole and displays the other {1 $\bar{1}$ 0 2} poles (orange circles) as well as the (0 0 0 1) (red triangle pointing down), {1 1 $\bar{2}$ 0} (green diamonds) and {$\bar{1}$ 1 0 1} (purple triangles) poles; the (1 1 $\bar{2}$ 0) zone (dashed line) runs through three different poles and is also the trace of a mirror (1 1 $\bar{2}$ 0) plane; (c) a slice of the ionic structure of the r-plane of sapphire (Al ions are in grey and O ions are in red or orange as they belong to 2 different planes as seen on the left and bottom lateral views) showing that the directions of intersections of the stable facets with the r-plane run along dense Al directions. (For interpretation of the references to colour in this figure legend, the reader is referred to the web version of this article.)

Table 1
Miller indices of the main relevant crystallographic planes of the sapphire structure, of their normal and of the common directions with the r- or c- plane [25].

Plane name	Plane (hkil)	Perpendicular direction [u v t w] (c/a = 2.73)	Direction of the edge shared with the r-plane	Direction of the edge shared with the c-plane
r	(1 $\bar{1}$ 0 2)	[47 $\bar{4}\bar{7}$ 0 19]	x	[1 1 $\bar{2}$ 0]
c	(0 0 0 1)	[0 0 0 1]	[1 1 $\bar{2}$ 0]	x
a	(1 1 $\bar{2}$ 0)	[1 1 $\bar{2}$ 0]	[19 $1\bar{9}$ 0 94] (almost [1 $\bar{1}$ 0 5])	p-facet in between
s	($\bar{1}$ 1 0 1)	[$\bar{5}$ 5 0 1]	[1 1 $\bar{2}$ 0]	r-facet in between
p	(1 1 $\bar{2}$ 3)	[33 33 $6\bar{6}$ 20]	[$\bar{1}$ 1 0 1]	[1 $\bar{1}$ 0 0]
None	($\bar{1}$ 1 0 5)	[$\bar{1}$ 1 0 1]	x	x

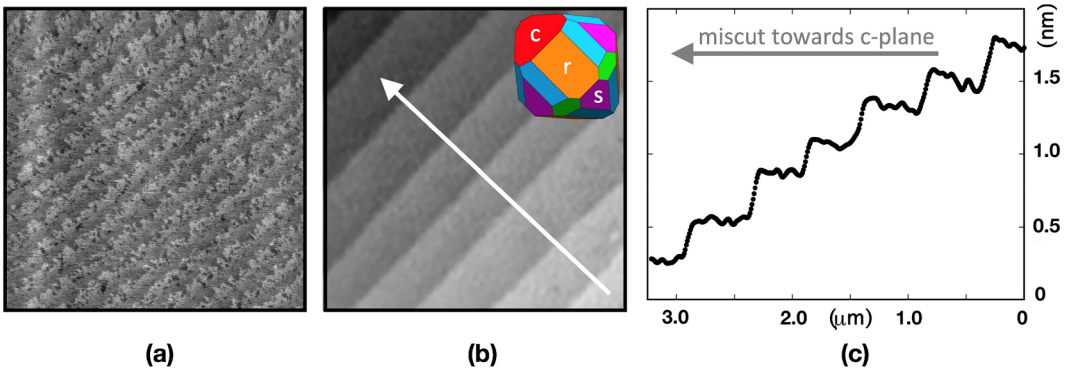

Fig. 2. (a and b) Topographic AFM images of the steps on the substrates: (a) 5 μm × 5 μm image after oxygen plasma treatment at 473 K; (b) 3 μm × 3 μm image after annealing in contact with the Ni film at 1423 K under Ar-H_2; the inset at the top right is the sapphire ECS positioned crystallographically parallel to the substrate within ± 5°, using the sapphire wafer flat cut as reference. The average step direction runs along a ⟨1 1 $\bar{2}$ 0⟩direction. (c) Step profile taken along the white arrow on (b) showing that the surface is miscut towards the c-plane (red facet at the top left of the ECS). (For interpretation of the references to colour in this figure legend, the reader is referred to the web version of this article.)

of the r-sapphire surface morphology after the oxygen plasma treatment. The surface consists of large "blurred" terraces about 450 ± 50 nm wide separated by 0.30 ± 0.03 nm high steps, i.e. the wafer surface is miscut off the r-plane by 0.04°, and is tilted by an angle 20 times larger than the curvature defect of the wafer. Fig. 2b shows the typical sapphire surface, found on a dewetted region, after annealing at 1423 K (0.83 T_mNi) in contact with a Ni film. Interfacial diffusion of sapphire has reshaped the substrate into atomically flat terraces with well-defined edges and no width change. The observed step height of 0.33 ± 0.03 nm is consistent with the nominal value of 0.35 nm expected for the r-plane of sapphire. Comparison of the AFM image in Fig. 2b with the sapphire ECS inset shows that the initially blurred edges of the terraces have straightened out along the [1 1 $\bar{2}$ 0] direction (within ± 5°). Fig. 2c is a profile taken along the arrow in Fig. 2b. It

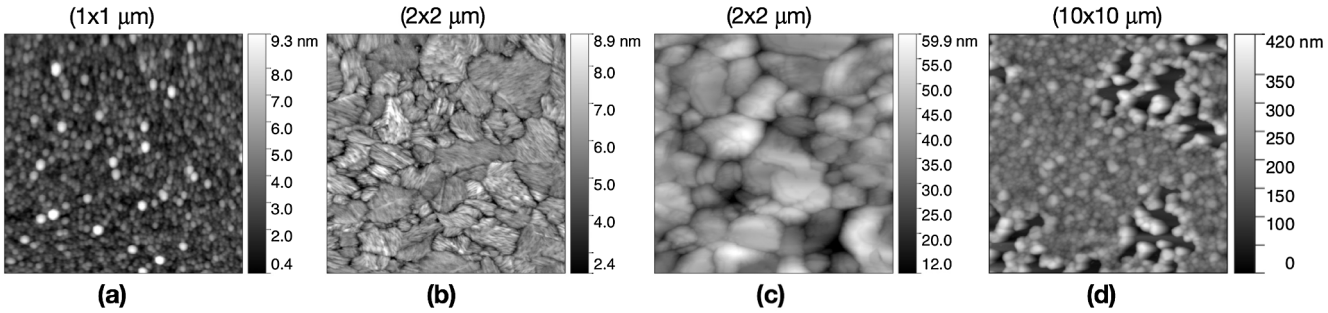

Fig. 3. AFM images of a polycrystalline 100 nm thick Ni film after successive anneals (note that the images have different fields of view; areas are indicated above each image). The grey levels of the vertical bar on the right side of each image show the relative height of the surface. In (a), (b) and (c) the grey levels correspond to the Ni surface heights; in (d), the darkest level is the sapphire substrate. (a) 1 μm × 1 μm image of an as-deposited film with grains about 30 nm wide; (b) 2 μm × 2 μm image after annealing at 773 K (0.45 T_mNi) for 1 h; (c) 2 μm × 2 μm image after an additional hour of annealing at 873 K (0.51 T_mNi); (d) 10 μm × 10 μm image after an additional 30 min of annealing at 1073 K (0.62 T_mNi).

shows that the sapphire substrate has been miscut towards the c-plane.

4.2. Ni film stability and grain growth

Two significantly different behaviors of the Ni films were observed upon annealing, depending on their thickness. The *thinner* films (~100 nm thick) break up into micron size islands once their grains have reached a size of about 5–10 times the film thickness, whereas the *thicker* films (with thicknesses ranging from 295 to 560 nm) undergo grain growth to sizes of up to 300 times larger than their thickness.

4.2.1. Thinner Ni films

Fig. 3 presents a series of AFM images, which illustrate the evolution of the microstructure of a *thinner* 100 nm thick Ni film after successive anneals at temperatures between 773 K (0.45 T_mNi) and 1073 K (0.62 T_mNi).

After 1 h at 773 K (0.45 T_mNi), the as-deposited Ni nano-grains (Fig. 3a) have coarsened to reach a size of 200–500 nm (Fig. 3b), i.e. 2–5 times the thickness of the film. The surface roughness of the film remains identical to its initial roughness, i.e. with an amplitude of less than 10 nm. This means that grain coarsening/growth is the dominant process that operates during this first annealing step, as previously reported [27,28]. An additional hour of annealing at 873 K (0.51 T_mNi) (or 973 K (0.56 T_mNi)) barely changes the grain size, but significantly increases the surface roughness by a factor of 10, as shown in Fig. 3c, due to grain boundary (GB) and triple junction grooving. The groove depth reaches a maximum of 80 nm, i.e. is almost equal to the film thickness. Such a morphology develops by Ni surface diffusion in order to balance the interfacial tensions at the intersections of the GBs with the surface, and to decrease the curvature gradient at the grain surfaces towards a constant curvature [29]. Grooving of the GBs pins them and almost stops coarsening once the grain size has reached about 2–5 times the film thickness. During a further 30 min anneal at 1073 K (0.62 T_mNi), grains have grown somewhat, up to sizes of between 500 nm and 1 μm, and grooving has continued, see Fig. 3d. Several groove roots have reached the sapphire substrate (black regions), and holes in the film have begun to expand. If we assume a dihedral angle of 17° for general GBs (i.e. for GBs with an energy of one third of the surface energy [30]), 1 μm diameter grains in a 100-nm thick film cannot reach a stable configuration before the root of the groove reaches the substrate. Further annealing at higher temperature, and/or for longer times, produces the complete breakup of the film into islands. The Ni film has completely broken up into 1–5 μm single crystal islands after annealing at 1423 K (0.83 T_mNi) for one hour.

The contact angle of the Ni crystals formed after dewetting is larger than 90° as observed in SEM images. Analysis of the AFM profiles of six grains with sizes ranging from 1.5 to 3 μm, and with shapes approximating a truncated sphere, provides an estimate for this angle of 129 ± 6°, which is consistent with the value measured for Ni crystals equilibrated on sapphire under H_2 at 1623 K (0.94 T_mNi) (119 ± 1°) [11].

4.2.2. Thicker Ni films

In a second set of experiments, *thicker* nickel films have been annealed around 1423 K (0.83 T_mNi). Higher temperature enhances the kinetics of grain growth, and thicker films favor unpinning of the GBs from their grooves at the film surface because the ratio of the groove depth to grain boundary height is relatively small.

While the literature claims that film grain size is limited to *10–20 times* film thickness (see for example [28,31]), the grains of the *thicker* Ni films annealed at 1423 K (0.83 T_mNi), have grown up to 100 μm, i.e. up to 300 times larger than the thickness of the film, as shown in Fig. 4a and b for films 295 and 560 nm thick, respectively. Some grains within a given film have undergone abnormal growth and are much larger than the others. These larger grains often have a free edge, i.e. they are located either at the periphery of the film or at the edges of dewetted regions.

Since similar microstructures are obtained after 1 or 2 h of annealing at 1423 K (0.83 T_mNi) it is concluded that grain growth takes place within the first hour of annealing. Similar rapid grain growth at the very beginning of annealing has also been reported during in-situ observation of 40 nm thick Ag films on silica at 603 K (0.49 T_mAg) [32] and Al films on silica at 723 K (0.77 T_mAl) [33].

Fig. 4c and d show the details of the surface morphology of the film after grain growth. As will be shown below, these two regions of a 560 nm film have a ⟨1 1 1⟩ direction perpendicular to the substrate surface, which will be referred to as a ⟨1 1 1⟩ texture later on. The bumps at the grain surfaces in Fig. 4c correspond to the ghosts of small grains that have been absorbed by the growth of larger ones. Fig. 4d shows a small isolated grain (marked by an arrow) with its equilibrium curvature and a tilted facet (i.e. it is not ⟨1 1 1⟩ textured) that has been trapped among large ⟨1 1 1⟩ textured grains.

4.3. Orientation relationships of Ni grains on the r-sapphire substrate

The orientations of the Ni grains in the film and of the underlying sapphire substrate were determined by automated EBSD mapping in a SEM. The film and the substrate of each sample were analyzed during a single experimental run. This ensures an accuracy of the relative orientation between two crystals of better than 0.3°. In addition, the absolute error of measurement due to sample positioning in the microscope can be corrected since the substrate orientation is known. The orientation relationships (ORs) between the Ni grains and the sapphire substrate were determined by comparing the pole figures (PFs) and/or the stereograms of the two phases obtained from the EBSD data, as described in a previous paper [17]. Two microscopes were employed in this study. One was located at CEMEF in Sophia-Antipolis, France: a

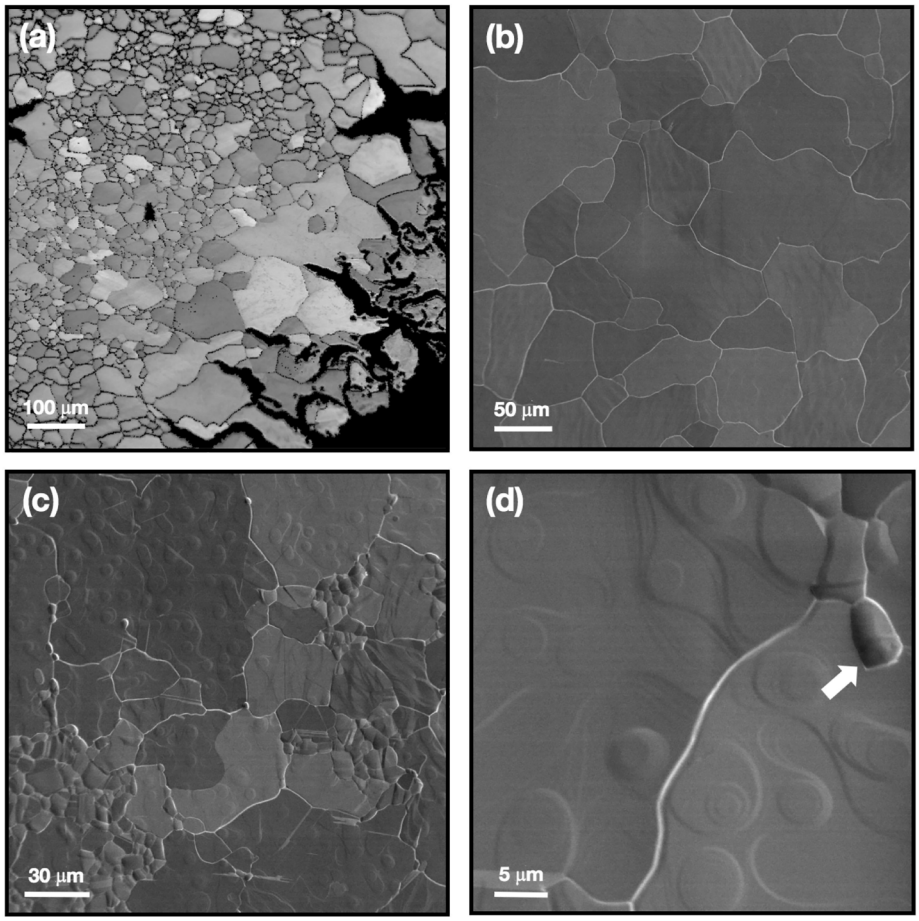

Fig. 4. Microstructure of the Ni films at different magifications. (a) Typical grain distribution taken from an EBSD scan of a 295 nm thick Ni film after successive anneals for about 1 h at temperatures culminating at 1423 K. Black regions are dewetted substrate zones. The largest grains lie at film free edges. (b–d) UHV-SEM back-scattered electron images of a 560 nm film after two successive anneals at 1423 K (0.83 T_mNi) for 1 h and 2 h; (b) Typical grain size distribution; (c and d) details of the surface topology of large grains oriented with ⟨1 1 1⟩ perpendicular to the substrate surface grown at the expense of smaller ones.

Zeiss Supra 40 SEM, equipped with a field emission gun (FEG) and a combined QUANTAX EDS/EBSD system from the Bruker company, including an EDS XFlash 5030 detector and an e$^-$Flash^{HR} EBSD detector, controlled by the ESPRIT software package, where the EBSD data were post-processed with the TSL/EDAX OIM software package. The other microscope was located at Carnegie Mellon University in Pittsburgh, PA, USA: a FEI Quanta 200 FE ESEM equipped with an EDAX/TSL orientation system and the Hikara high speed EBSD detector. Data were acquired at 20 or 30 kV with the substrate plane tilted by 70° with respect to the electron beam. Since carbon coating degrades the EBSD signal, the sample was grounded to the sample holder either with silver paste or with aluminum foil tightly connected to the Ni film by a screw to ensure good electrical contact. The latter method of grounding allowed the samples to undergo subsequent additional annealing without the risk of contamination. The sapphire orientation of each sample was acquired on a region where the substrate was free of Ni deposit.

Below, we present the orientations adopted by Ni grains in *thicker* and *thinner* films processed on two sapphire substrates cut from the same wafer, i.e. having the same terraces and steps. We first describe the non-random ORs within a ⟨1 1 1⟩ textured 295 nm thick Ni film annealed at 1423 K (0.83 T_mNi) for one hour. Then we present the ORs of grains grown in a 100 nm thick film, which began to break-up at 1073 K (0.62 T_mNi). These ORs illustrate the process of evolution from an untextured nano-polycrystalline to a textured film.

4.3.1. *Thicker Ni films*

Polycrystalline Ni films of thickness between 295 nm and 560 nm develop a ⟨1 1 1⟩ texture when annealed at 1423 K (0.83 T_mNi) for one or two hours. X-ray diffraction of one sample showed that the {1 1 1} interfacial planes of the Ni grains were parallel to the $(1\ \bar{1}\ 0\ 2)$ plane of sapphire within less than 0.2°.

Fig. 5 describes the results of EBSD analysis of a 295 nm thick film. Fig. 5a is a 480 × 500 μm large-scale map scanned with a 2 μm step over a hexagonal grid, which displays colored Ni grains and black sapphire regions (~9% of the map area) from which the Ni film has undergone dewetting. The average grain size is 43 μm with a standard deviation of 13 μm. The largest grain has reached a size of 95 μm. Ni grains are colored according to four major ORs on the sapphire substrate. Grains colored in darker blue and in red correspond to grains with ORs which we will refer to as OR1r and OR2r, respectively, and those colored in light blue and pink correspond to twin variants of OR1r and OR2r, which we will refer to as OR1r/t and OR2r/t, and which are rotated by 60° (or 180°) about the ⟨1 1 1⟩ axis perpendicular to the film surface, respectively. These ORs are described in greater detail below. Ni grains colored in grey in Fig. 5a, occupy 4.5% of the Ni grain area, and deviate from the major ORs by more than 5°.

Fig. 5b is a PF of the Ni grains centered on the (1 1 1) pole showing the distribution of the {1 1 0} poles. This Ni PF has been rotated about its ⟨1 1 1⟩ central axis such that the sapphire stereogram of Fig. 5c, obtained using the EBSD data acquired during the same run, is aligned with the sapphire stereogram of Fig. 1b. Fig. 5c is a simplified copy of Fig. 1b, and is reproduced here for convenience of comparison with other components of Fig. 5. Superimposition of the plots of Fig. 5b and c allows the determination of the four major ORs adopted by the Ni grains on the r-sapphire.

Fig. 5d–g are the stereograms of the Ni grains with the four different observed ORs: OR1r, OR1r/t, OR2r and OR2r/t, respectively. The color code of their backgrounds is the same as in Fig. 5a. They are centered on the (1 1 1) pole and display the {1 1 1}, {1 0 0} and {1 1 0} poles together with the zone of the $(1\ \bar{1}\ 0)$ pole (dashed line).

Fig. 5d corresponds to the preferred OR, namely OR1r. The zone of the Ni$(1\ \bar{1}\ 0)$ pole is parallel to the zone of the $(1\ 1\ \bar{2}\ 0)$ pole of the

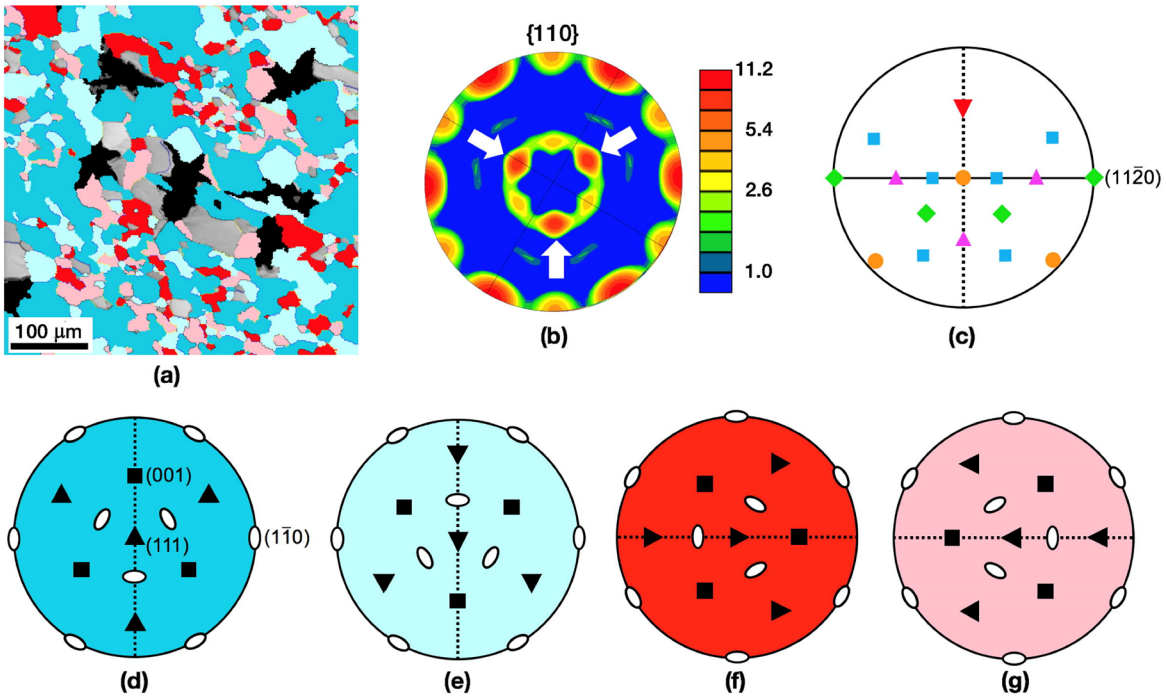

Fig. 5. EBSD data of one representative 480 × 500 µm region of a 295 nm thick Ni film on a r-sapphire substrate annealed up to 1423 K (0.83 T_mNi). (a) Map of the Ni grains colored according to their ORs on the substrate with a tolerance angle of ± 5°; in the black regions the Ni film is dewetted; (b) PF of the Ni grains showing the distribution of the {1 1 0} poles. The intensities are given in multiples of a random distribution (MRD); the white arrows mark the {1 1 0} poles which belong to the preferred OR; (c) sapphire stereogram oriented as Fig. 1b for comparison with Fig. 5d–g. (d–g) Stereograms of nickel centered on a (1 1 1) pole on which are located other {1 1 1} poles (triangles) as well as the {1 0 0} (squares) and the {1 1 0} (ovals) poles. They are oriented with respect to the sapphire stereogram of (c) in OR1r, OR1/t, OR2r and OR2r/t, respectively. The dashed lines in (d) to (g) identify the zone of the (1 $\bar{1}$ 0) pole which is also the trace of a mirror (1 $\bar{1}$ 0) plane.

sapphire stereogram of Fig. 5c. Fig. 5d has six {1 1 0} poles on the outer circle and three more at 35° from the center (those marked by white arrows in Fig. 5b), which correspond to the nine more intense {1 1 0} poles of the nickel PF of Fig. 5b. Two of the {1 1 0} poles on the outer circle of Fig. 5b and 5d correspond, within ± 5°, to the two {1 1 $\bar{2}$ 0} poles of sapphire (green squares) on the outer circle of the sapphire stereogram of Fig. 5c. Since two opposite poles on the outer circle of a stereogram of a PF define a direction within the interfacial plane, OR1r may be written as follows:

$$OR1r = Ni(1\,1\,1)[1\,\bar{1}\,0]//\alpha\text{-}Al_2O_3(1\,\bar{1}\,0\,2)[1\,1\,\bar{2}\,0]$$

The light blue Ni grains in Fig. 5a, which are in twin orientation to the darker blue grains, have the OR1r/t orientation relationship. Their stereogram, shown on Fig. 5e, has the same six {1 1 0} poles on the outer circle of Fig. 5b as the ones originating from the OR1r grains, as well as the three lower intensity {1 1 0} poles at 35° from the center, that are rotated by 180° (or 60°) from the most intense poles. OR1r/t is half as frequent as OR1r, as indicated by the intensities of the poles at 35° from the center of the PF of Fig. 5b.

The secondary OR, referred to as OR2r, corresponds to the red grains of the map of Fig. 5a and to the stereogram of Fig. 5f. The six {1 1 0} poles on the outer circle of Fig. 5f correspond to the six weaker ones of the PF of Fig. 5b, which are rotated by 90° from the ones belonging to the OR1r grains. The zone of the (1 $\bar{1}$ 0) pole is parallel to the ($\bar{1}$ 1 0 5) zone (horizontal solid line in the sapphire stereogram of Fig. 5c), i.e. a dense ⟨1 1 0⟩ direction within the (1 1 1) interfacial plane of Ni is parallel to the [$\bar{1}$ 1 0 1] direction in the r-plane of sapphire (see Fig. 1 and Table 1). This OR may be written as follows:

$$OR2r = Ni(1\,1\,1)[1\,\bar{1}\,0]//\alpha\text{-}Al_2O_3(1\,\bar{1}\,0\,2)[\bar{1}\,1\,0\,1]$$

Pink Ni grains, twins of the red grains, are in OR2r/t, which is illustrated in Fig. 5g. Red/pink twinned grains occupy equivalent surface fractions, and are half as frequent as those with OR1r. These frequencies have been measured from the PF of the distribution of the {1 1 1} poles of Ni (not shown here), and are consistent with the surface fractions occupied by each type of grain on Fig. 5a.

The largest Ni grains (darker blue in Fig. 5a) are oriented according to OR1r. The grains with OR1r/t, OR2r and OR2r/t are smaller.

Finally, by superimposing the sapphire and the four Ni stereograms, it is observed that OR1r and OR1r/t represent different orientation relationships, while OR2r and OR2r/t are identical because the (1 1 $\bar{2}$ 0) plane of the substrate and the (1 $\bar{1}$ 0) plane of the Ni are mirror planes.

4.3.2. *Thinner Ni films*

The *thinner* 100 nm Ni films did not grow into large grains before breaking-up at temperatures as low as 1073 K (0.62 T_mNi), as shown in Fig. 6a, which is an EBSD map of a representative region of the sample. At the top right of the image, there is a dewetted region (marked by a white cross) that has been used to identify the sapphire substrate orientation. The black regions surrounding the dewetted zone, or scattered within the map, are not holes in the film but curved regions in the Ni film where the electron beam is shadowed so that orientations cannot be determined [34]. The average grain size is 450 nm with a standard deviation of 150 nm. A few grains have reached the maximum size of about 900 nm. The grains are colored depending on their interfacial plane orientation according to the key provided by the standard stereographic triangle (SST) for a fcc crystal displayed as an inset on the image. The film is not as completely ⟨1 1 1⟩ textured as was the thicker film annealed at higher temperature, described in the previous section. However, the dark blue Ni grains, which have a {1 1 1} interfacial plane, are the most frequent and the largest ones; within a 5° tolerance, the {1 1 1} interfacial plane is 8 times more frequent than random, as indicated in Fig. 6b, which shows the distribution of the interfacial Ni planes parallel to the sapphire substrate in the form of an inverse pole figure (IPF).

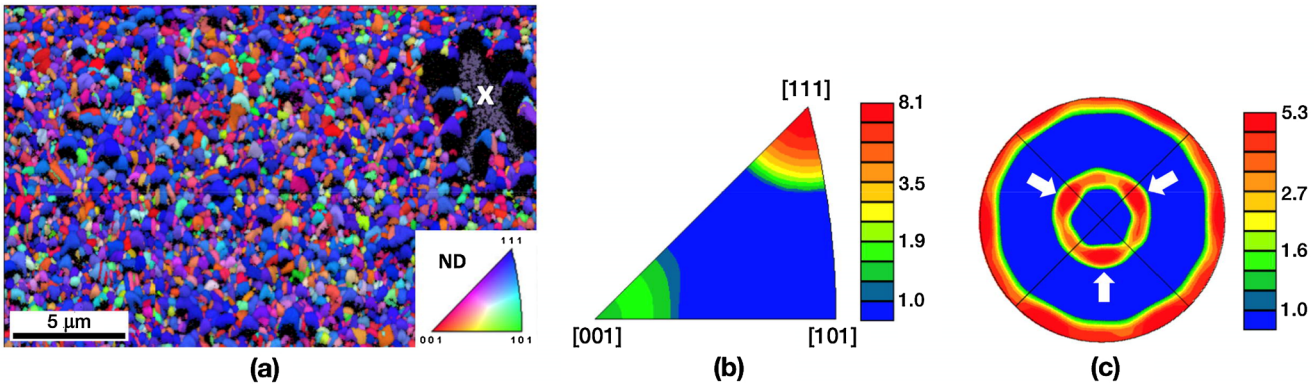

Fig. 6. (a) 30 × 20 μm EBSD map, scanned with a 35 nm step, of a representative region of a 100 nm *thinner* Ni film annealed at temperatures up to 1073 K (0.62 T_mNi). The grain colors correspond to their sample surface normal direction (ND), i.e. interfacial plane orientation, according to the key shown on the SST in the inset; (b) Inverse pole figure of the sample surface normal direction showing the distribution of the Ni interfacial planes on the r-sapphire plane; the (1 1 1) planes are the most frequent; (c) {1 1 0} PF of the Ni grains with a (1 1 1) plane parallel to the sapphire substrate with a tolerance of 5°. The white arrows identify some of the {1 1 0} poles of the preferred OR. The scale bars in (b) and (c) are in units of MRD.

Fig. 6c is the {1 1 0} PF of the Ni grains with a {1 1 1} plane parallel to the r-sapphire substrate showing the distribution of their {1 1 0} poles; these grains have been selected from the normal direction IPF plotted in Fig. 6b, with a tolerance of 5° from (1 1 1). Fig. 6c has been rotated such that the sapphire substrate stereogram of the Ni film is oriented parallel to the sapphire stereogram illustrated in Fig. 1b (and in Fig. 5c). The stereogram of the Ni grains with the most frequent OR is the same as that shown previously in Fig. 5d, i.e. these grains are in OR1r; they have the nine most intense {1 1 0} poles of Fig. 6c, six of which lie on the outer circle, and three of which are located at 35° from the (1 1 1) center and are highlighted by white arrows. Thus, at this stage of annealing (1073 K (0.62 T_mNi)), the Ni grains with OR1r in this *thinner* film have already grown bigger at the expense of the grains with different ORs. The other three ORs identified for *thicker* films, i.e. OR1r/t and both OR2r and OR2r/t, are also present, but with frequencies lower than those found for OR1r.

4.4. Orientation relationships of the grains of a Cu film on the r-sapphire substrate

Here, it is relevant to present the results obtained on a *thicker* copper film on the r-plane of sapphire, prepared under similar conditions to those used for the nickel films. A nano-crystalline 730 nm thick Cu film, annealed at 1253 K (0.92 T_mCu) for 78 h was found to have developed a ⟨1 1 1⟩ texture with very large grains, exceeding several hundreds of microns, as well as some marginal dewetted regions. The initial nano-structure of the film was identical to that of the Ni films shown in Fig. 3a, as determined by AFM.

Fig. 7a is a 1.5 mm × 1.4 mm EBSD map of a representative region of the Cu film scanned with a 10 μm step. The majority of Cu grains adopt the same four ORs as those found for Ni grains in *thicker* films; thus the Cu grains of Fig. 7a have been colored using the same scheme as that used for the Ni film presented in Fig. 5a (Cu grains in OR1r in darker blue, their twins in OR1r/t in light blue, grains in OR2r in red and their twins in OR2r/t in pink). The dewetted regions, colored black, cover 13% of the map. Grains colored in grey are ones that deviate from the four major ORs by more than 5°; they represent 18% of the grain area. Fig. 7b is a PF of Cu centered on the (1 1 1) pole showing the distribution of the {1 1 0} poles of all Cu grains and positioned such that the sapphire substrate stereogram in this case is also parallel to the one shown previously in Fig. 1b (or Fig. 5c). OR1r/t (light blue grains) is slightly preferred over OR1r (10% more occurrences) and is twice as frequent as OR2r or OR2r/t. The stereogram of the Cu grains which display the majority orientation relationship with the substrate, namely OR1r/t, is identical to the one plotted for Ni in Fig. 5e.

Fig. 8a is an AFM image of the sapphire substrate after annealing in contact with the Cu film. The inset in the top right hand corner of Fig. 8a is a sketch of the sapphire ECS oriented crystallographically parallel to the substrate. Fig. 8a shows that the sapphire substrate has 830 ± 30 nm wide r-plane terraces with steps running along the same [1 1 $\bar{2}$ 0] direction as in the substrates used for the Ni films. However, Fig. 8b which is a profile along the white arrow drawn on Fig. 8a shows that the miscut of this r-sapphire substrate is towards the {$\bar{1}$ 1 0 $\bar{1}$} s-plane of sapphire (purple facet on the ECS) i.e. it is miscut in the opposite direction from that of the substrates used for the Ni films, which was towards the (0 0 0 1) plane (red facet).

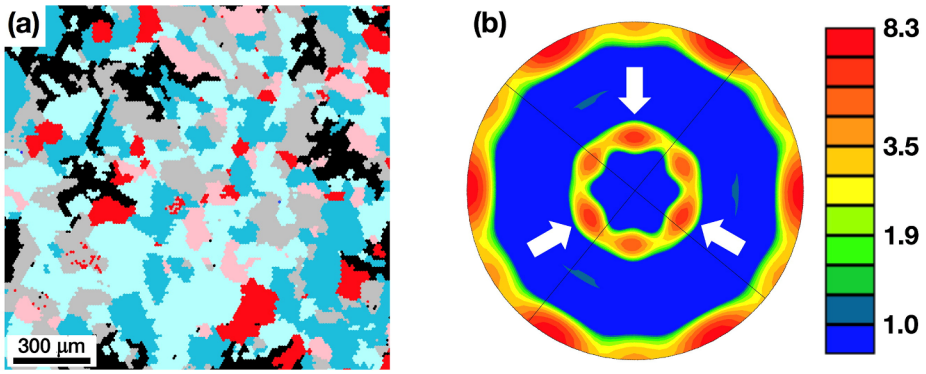

Fig. 7. Data from a thick Cu film annealed on the r-plane of sapphire: (a) 1.5 mm × 1.4 mm EBSD map scanned with a 10 μm step, where the grains are colored according to their orientation relationship on the sapphire (see text); (b) {1 1 0} PF of the Cu grains, showing the distribution of the {1 1 0} poles (units are in MRD); arrows mark the poles of the preferred OR (corresponding to OR1r/t).

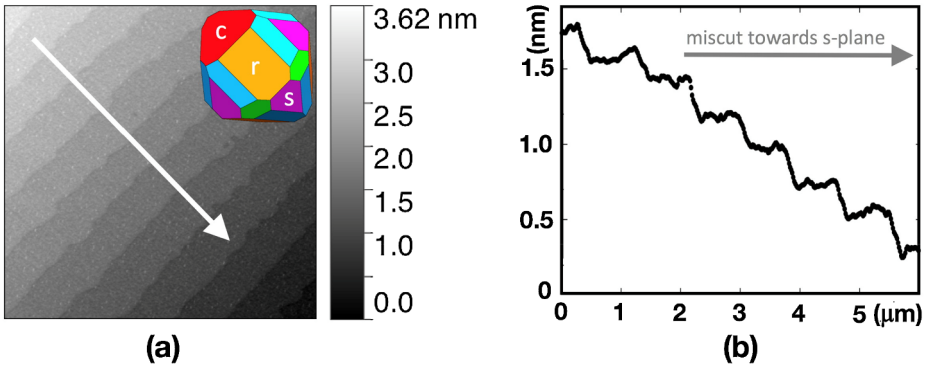

Fig. 8. (a) AFM image (7 μm × 7 μm) of the sapphire substrate with the ECS sapphire inserted at the top right, and positioned crystallographically parallel to the substrate; (b) step profile taken along the white arrow in (a) showing that the surface is miscut towards the s-plane (purple facet of the ECS). (For interpretation of the references to colour in this figure legend, the reader is referred to the web version of this article.)

5. Discussion

5.1. Grain growth, film thickness and orientation relationships

Most of the studies that have addressed the microstructure of annealed thin polycrystalline fcc metallic films on oxides have been performed on amorphous substrates, i.e. silica [see for example Refs. 31,32,35,36]. They focus on thin films with thicknesses that range from a few tens to 100 nm, and they address either the mechanisms of dewetting or of stagnation of grain growth at sizes of 10–20 times the thickness of the film [28,31,37].

Our experiments on Ni and Cu films on a r-sapphire surface show that it is possible to grow ⟨1 1 1⟩ textured films from a randomly oriented nano-crystalline microstructure, with grains that are much larger than usually expected from experiments conducted on amorphous substrates. Given a film thickness that is large enough (i.e. more than 300 nm for Ni films), Ni grains grow to sizes as large as 300 times the thickness of the film, at an annealing temperature of about 83% of the Ni melting point. Cu grains grow even larger, about 500 times the thickness of the film, when annealed at a higher equivalent temperature (of about 92% of its melting point).

These differences between the behavior of films on amorphous versus crystalline substrates may have a simple explanation. On an amorphous substrate the surfaces of all grains in a textured film have approximately the same orientation so that their surface as well as their interfacial energies should all be similar. Therefore, there is little driving force available for growth of one grain at the expense of others, except for the elimination of grain boundaries. In contrast, for a textured film on a crystalline substrate, while the surface energies of film grains may all be similar, different grains will have different in-plane orientations on the substrate, and there will be a driving force available for growth of grains with low interfacial energy at the expense of those with higher interfacial energy [38]. There may, of course, also be other factors at play, such as grain size and GB mobility.

Deep grooving of the GBs down to the substrate is responsible for the break-up of the thinnest films into single-crystalline islands before the grains have had an opportunity to grow to sizes larger than 10 times the thickness of the film. Dewetting by the formation of holes can occur before a film has achieved a fiber texture. This is what has been observed here for the thinnest 100 nm Ni films. Once separated from the grains of lowest interfacial energy, which can expand by grain growth, isolated 100 nm grains of higher interfacial energy, with diameters of the order of one micron, cannot easily rotate so as to achieve low interfacial energy.

5.2. Possible origin of the orientation relationships

The majority of the grains in thicker Ni films on r-plane sapphire adopt an OR1r orientation relationship, in which a Ni {1 1 1} plane is parallel to the sapphire r-plane and a Ni ⟨1 1 0⟩ direction in the interface lies parallel to a sapphire [1 1 $\bar{2}$ 0] interface direction. In contrast, the principal OR adopted by a thick Cu film is OR1r/t. In this case also, a Cu {1 1 1} plane is parallel to the sapphire r-plane and a Cu ⟨1 1 0⟩ direction lies parallel to a sapphire [1 1 $\bar{2}$ 0] direction. The difference between the two cases is that for the Ni film, the sapphire substrate was miscut towards the c-plane, whereas the Cu film was grown on a sapphire substrate that was miscut towards the s-plane. Thus, it is interesting to address one other issue regarding these two ORs. On the metal film side of the interfaces, edges that run in a ⟨1 1 0⟩ direction may connect a {1 1 1} interfacial terrace plane to two different kinds of ledges: either a ledge with a {1 0 0} surface plane or one with a {1 1 1} surface plane. If we consider the relative orientations of OR1r for Ni (Fig. 5d) with the corresponding sapphire substrate orientation (Fig. 5c) it should be clear that, for a case where the miscut of the sapphire surface is tilted towards the c-plane (red triangle pointing down in Fig. 5c), the ledge on the metal side will have a {1 0 0} surface facing the (0 0 0 1) c-plane ledge. Similarly, for Cu with an OR1r/t (Fig. 5e) on a miscut sapphire surface tilted towards the (1 $\bar{1}$ 0 $\bar{1}$) s-plane (purple triangle in Fig. 5c) the ledge on the Cu side of the interface will also have a {1 0 0} surface facing the s-plane. One may conclude from these observations that a {1 0 0} ledge surface is the preferred orientation on the metal side for both the Ni and Cu films, thereby leading to different ORs in each case. Thus, the accommodation of the ledge-ledge interaction across the interface plays a non-negligible role in the determination of the preferred OR.

Another possible interpretation of the observed ORs is due to Fecht and Gleiter [15], who hypothesized that the lowest energy OR between a metal and an ionic substrate is achieved when the dense directions within the interfacial planes of the two phases are aligned. However, this hypothesis does not agree with the fact that the densest direction in the r-plane of sapphire is the [1 $\bar{1}$ 0 1] direction [39], which is perpendicular to the [1 1 $\bar{2}$ 0] sapphire direction with which the close packed ⟨1 1 0⟩ directions of Ni and Cu are observed to align here. Furthermore, the Fecht and Gleiter hypothesis is based on a lattice mismatch argument, which is improbable given that the interfaces between the metal/sapphire couples we have studied here are most likely to be incoherent.

It is also instructive to examine the ORs of metallic fcc films on other sapphire substrate orientations, and in particular on the most widely studied (0 0 0 1) c-plane of sapphire, in the framework of interfacial steps. Most of the papers [1–14] report a preferred OR1c: Me(1 1 1)[1 $\bar{1}$ 0]//α-Al_2O_3(0 0 0 1)[1 $\bar{1}$ 0 0], where Me = Al, Cu, Ni or Pt. However, when samples are prepared at high temperature (by sintering for Cu [8], or annealing for Al films [1]), another OR, OR2c, becomes preferred. OR2c: Me(1 1 1)[1 $\bar{1}$ 0]//α-Al_2O_3(0 0 0 1)[1 1 $\bar{2}$ 0], is rotated by 30° (or 90°) from OR1c. A TEM study of the impact of steps on the OR of Cu crystals on the c-plane of sapphire showed that the step edge directions determine the ORs [9]: OR1c and OR2c are found when the step edges run along sapphire ⟨1 $\bar{1}$ 0 0⟩ and ⟨1 1 $\bar{2}$ 0⟩ directions, respectively.

An interpretation of the above observations can also be provided by considering the effects of substrate step orientation on film ORs. Fig. 9a shows the Wulff shape of a completely facetted crystal of sapphire,

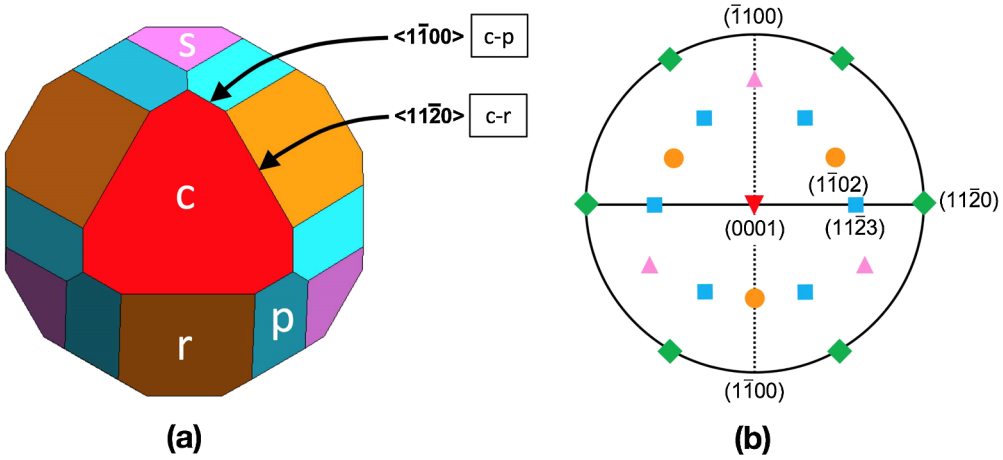

Fig. 9. (a) Fully facetted ECS of sapphire viewed along a direction perpendicular to the c-plane (same color code as in Fig. 1a); the 6 (green) a-facets shown in (b) are perpendicular to the c-facet, and therefore not seen in (a). Around the c-plane, 3 step edges run along [1 $\bar{1}$ 0] directions (intersections with the 3 r-planes) and 6 step edges run along [1 $\bar{1}$ 0 0] directions (intersections with the 6p-planes); (b) Corresponding sapphire stereogram; the (1 1 $\bar{2}$ 0) zone (dashed line) runs through three different poles while the ($\bar{1}$ 1 0 0) zone displays a mirror symmetry about the c-pole at the center. (For interpretation of the references to colour in this figure legend, the reader is referred to the web version of this article.)

similar to the one displayed in Fig. 1a, but viewed along the [0 0 0 1] direction. If a c-plane sapphire crystal is miscut towards the r-plane, the step edges would run in a ⟨1 1 $\bar{2}$ 0⟩ direction and the metal film would display OR2c. In contrast, a c-plane-oriented crystal miscut in the opposite direction, i.e. towards the two p-planes, would possess ⟨1 $\bar{1}$ 0 0⟩ step edges and display OR1c. The observation of a switch from a predominant OR1c after relatively low temperature annealing, to a predominant OR2c following higher temperature treatment, could be the result of a small change in the Wulff shape of Fig. 9a with increasing temperature, which produced a relative expansion of the r-plane at the expense of the p-plane. Such a change could lead to the appearance of some ⟨1 1 $\bar{2}$ 0⟩ step edges on crystals randomly miscut and favor the development of OR2c.

Fig. 9b is the stereogram corresponding to Fig. 9a. Superimposition of the fcc stereograms of Fig. 5d–g, viewed along the ⟨1 1 1⟩ direction, onto the sapphire stereogram of Fig. 9b, will produce ORs corresponding to OR2c, OR2c/t, OR1c and OR1c/t, respectively. In their experiments on the Al/c-sapphire couple, Heike et al. [1] observed a preference for OR2c, together with some OR2c/t, over OR1c and OR1c/t, which have a similar abundance. Based on the superposition of the stereograms of Fig. 5d–g in Fig. 9b, we would expect OR1c and OR1c/t to have identical abundance (as the stereogram superpositions produce mirror related patterns), whereas the abundances of OR2c and OR2c/t should be different. Thus, those results [1] are also consistent with our present analysis.

The interpretations proposed here to explain the ORs of fcc films on r-sapphire have relied on the presumed existence of a strong influence of surface step edges on the development of film orientation. Extending similar concepts to previous observations of fcc films equilibrated on c-plane sapphire substrates has also produced interesting conclusions. These ideas therefore deserve additional experiments on films grown on substrates that have been deliberately miscut in different directions, so as to produce different types of surface step edges, in order to verify the manner in which step edges affect the final film ORs.

6. Summary

When nano-crystalline nickel films, about 100 nm in thickness, are annealed on the r-plane of sapphire, at temperatures of up to 1073 K, they tend to break up and dewet by the time their grains have grown to about 10 times the film thickness. Thicker Ni and Cu films, 300 or more nm in thickness, are more resistant to dewetting and can undergo grain growth to sizes that can exceed 300 times their film thickness. This grain growth is several tens of times larger than the stagnating grain size reported for experiments conducted with metallic films on amorphous substrates. In the present experiments, grain growth is driven by the anisotropic interfacial energy. Upon annealing, the films develop a ⟨1 1 1⟩-fiber texture with preferred azimuthal orientations along the fiber. This feature is correlated with the growth of grains of the preferred OR in both Ni and Cu metallic films, as has been observed for fcc metallic films on the c-plane of sapphire. The preferred OR does not necessarily lead to the alignment of the closest packed metal direction with the closest packed direction in the substrate surface. Instead, the closest packed metal direction aligns with the direction of the substrate step edges that develop during annealing of the metallic film on the sapphire surface. In addition, the crystallographic asymmetry of the r-plane on each side of the ⟨1 1 $\bar{2}$ 0⟩ direction, has revealed that metal films can develop different ORs depending on the surface ledge orientations produced by the sapphire miscut. While the steps of the miscut sapphire have different ledge orientations, the fcc metals investigated prefer to develop with ORs that favor the same {1 0 0} rather than a {1 1 1} ledge surface orientation.

Finally, this paper has shown that very large thin grains can be grown on a substrate with poor lattice matching. It has also been shown that grain growth can be managed by choosing not only the orientation of the substrate, but the asymmetry that may result by changing the direction of its miscut.

Acknowledgments

The authors thank Alain Ranguis (CINaM, Marseille) for his assistance with AFM measurements. D.C. and B.C. wish to thank the Agence Nationale de la Recherche for support of their research under grant ANR-GIBBS-15-CE30-0016. Substrate preparation and nickel film deposition were performed in the PLANETE cleanroom facility (CINaM, Marseille). G.S.R. acknowledges use of the Materials Characterization Facility at Carnegie Mellon University supported by Grant MCF-677785.

References

[1] S.W. Hieke, B. Breitbach, G. Dehm, C. Scheu, Microstructural evolution and solid state dewetting of epitaxial Al thin films on sapphire (alpha-alumina), Acta Mater. 133 (2017) 356–366, https://doi.org/10.1016/j.actamat.2017.05.026.
[2] G. Dehm, B. Inkson, T. Wagner, Growth and microstructural stability of epitaxial Al films on (0001) [alpha]-Al_2O_3 substrates, Acta Mater. 50 (2002) 5021–5032, https://doi.org/10.1016/S1359-6454(02)00347-6.
[3] D.L. Medlin, K.F. McCarty, R.Q. Hwang, S.E. Guthrie, Orientation relationships in

heteroepitaxial aluminum films on sapphire, Thin Solid Films 299 (1997) 110–114, https://doi.org/10.1016/S0040-6090(96)09393-5.
[4] G. Katz, The epitaxy of copper on sapphire, Appl. Phys. Lett. 12 (1968) 161–163, https://doi.org/10.1063/1.1651935.
[5] P.J. Moller, Q. Guo, Growth of ultrathin films of copper onto [alpha]-Al_2O_3 (0001): mechanism and epitaxy, Thin Solid Films 201 (1991) 267–279, https://doi.org/10.1016/0040-6090(91)90116-F.
[6] D.W. Susnitzky, C.B. Carter, Metal particles on the surfaces of heat-treated ceramic thin films, Surf. Sci. 265 (1992) 127–138, https://doi.org/10.1016/0039-6028(92)90494-Q.
[7] H. Bialas, E. Knoll, Heteroepitaxy of copper on sapphire under UHV conditions, Vacuum 45 (1994) 959–966, https://doi.org/10.1016/0042-207X(94)90220-8.
[8] C. Scheu, M. Gao, S.H. Oh, G. Dehm, S. Klein, A.P. Tomsia, Bonding at copper–alumina interfaces established by different surface treatments: a critical review, J. Mater. Sci. 41 (2006) 5161–5168, https://doi.org/10.1007/s10853-006-0073-0.
[9] S.H. Oh, C. Scheu, T. Wagner, M. Ruhle, Control of bonding and epitaxy at copper/sapphire interface, Appl. Phys. Lett. 91 (2007) 141912, https://doi.org/10.1063/1.2794025.
[10] S. Curiotto, H. Chien, H. Meltzman, P. Wynblatt, G.S. Rohrer, W.D. Kaplan, D. Chatain, Orientation relationships of copper crystals on c-plane sapphire, Acta Mater. 59 (2011) 5320–5331, https://doi.org/10.1016/j.actamat.2011.05.008.
[11] H. Meltzman, D. Mordehai, W.D. Kaplan, Solid-solid interface reconstruction at equilibrated Ni-Al_2O_3 interfaces, Acta Mater. 60 (2012) 4359–4369, https://doi.org/10.1016/j.actamat.2012.04.037.
[12] G. Atiya, D. Chatain, V. Mikhelashvili, G. Eisenstein, W.D. Kaplan, The role of abnormal grain growth on solid-state dewetting kinetics, Acta Mater. 81 (2014) 304–314, https://doi.org/10.1016/j.actamat.2014.08.038.
[13] H. Zhou, P. Wochner, A. Schops, T. Wagner, Investigation of platinum films grown on sapphire (0001) by molecular beam epitaxy, J. Cryst. Growth 234 (2002) 561–568, https://doi.org/10.1016/S0022-0248(01)01676-1.
[14] S. Ramanathan, B.M. Clemens, P.C. McIntyre, U. Dahmen, Microstructural study of epitaxial platinum and permalloy/platinum films grown on (0001) sapphire, Philos. Mag. A 81 (2001) 2073–2094, https://doi.org/10.1080/01418610108216653.
[15] H.J. Fecht, H.A. Gleiter, Lock-in model for the atomic structure of interphase boundaries between metals and ionic crystals, Acta Metall. 33 (1985) 557–562, https://doi.org/10.1016/0001-6160(85)90019-7.
[16] P. Wynblatt, D. Chatain, Importance of interfacial step alignment in hetero-epitaxy and orientation relationships: the case of Ag equilibrated on Ni substrates. Part 1 computer simulations, J. Mater. Sci. 50 (2015) 5262–5275, https://doi.org/10.1007/s10853-015-9074-1.
[17] D. Chatain, P. Wynblatt, A.D. Rollett, G.S. Rohrer, Importance of interfacial step alignment in hetero-epitaxy and orientation relationships: the case of Ag equilibrated on Ni substrates. Part 2 experiments, J. Mater. Sci. 50 (2015) 5276–5285, https://doi.org/10.1007/s10853-015-9075-0.
[18] J. Wittkamper, Z. Xu, B. Kombaiah, F. Ram, M. De Graef, J.R. Kitchin, G.S. Rohrer, P.A. Salvador, Competitive growth of scrutinyite (α-PbO_2) and rutile polymorphs of SnO_2 on all orientations of columbite $CoNb_2O_6$ substrates, Cryst. Growth Des. 17 (2017) 3929–3939, https://doi.org/10.1021/acs.cgd.7b00569.
[19] M. Kitayama, A.M. Glaeser, The Wulff shape of alumina: III, Undoped alumina, J. Am. Ceram. Soc. 85 (2002) 611–622, https://doi.org/10.1111/j.1151-2916.2002.tb00140.x.
[20] J.H. Choi, D.Y. Kim, B.J. Hockey, S.M. Wiederhorn, C.A. Handwerker, J.E. Blendell, W.C. Carter, A.R. Rosen, Equilibrium shape of internal cavities in sapphire, J. Am. Ceram. Soc. 80 (1997) 62–68, https://doi.org/10.1111/j.1151-2916.1997.tb02791.x.
[21] M.A. van Hove, G.A. Somorjai, A new microfacet notation for high-Miller-index surfaces of cubic materials with terrace, step and kink structures, Surf. Sci. 92 (1980) 489–518, https://doi.org/10.1016/0039-6028(80)90219-8.
[22] M. Kitayama, A.M. Glaeser, The Wulff shape of alumina: IV. Ti4+-doped alumina, J. Am. Ceram. Soc. 88 (2005) 3492–3500, https://doi.org/10.1111/j.1551-2916.2005.00604.x.
[23] J.H. Choi, D.Y. Kim, B.J. Hockey, S.M. Wiederhorn, J.E. Blendell, C.A. Handwerker, Equilibrium shape of internal cavities in ruby and the effect of surface energy anisotropy on the equilibrium shape, J. Am. Ceram. Soc. 85 (2002) 1841–1844, https://doi.org/10.1111/j.1151-2916.2002.tb00362.x.
[24] R.V. Zucker, D. Chatain, U. Dahmen, S. Hagège, W.C. Carter, New software tools for the calculation and display of isolated and attached interfacial-energy minimizing particle shapes, J. Mater. Sci. 47 (2012) 8290–8302, https://doi.org/10.1007/s10853-012-6739-x.
[25] W.E. Lee, K.P.D. Lagerlof, Structural and electron diffraction data for sapphire (α-Al_2O_3), J. Electron Microsc. Tech. 2 (1985) 247–258, https://doi.org/10.1002/jemt.1060020309.
[26] P.S. Maiya, J.M. Blakely, Surface self-diffusion and surface energy of nickel, J. App. Phys. 38 (1967) 698–704, https://doi.org/10.1063/1.1709399.
[27] C.R.M. Grovenor, H.T.G. Hentzell, D.A. Smith, The development of grain structure during growth of metallic films, Acta metall. 32 (1984) 773–781, https://doi.org/10.1016/0001-6160(84)90150-0.
[28] H.J. Frost, C.V. Thompson, D.T. Walton, Simulation of thin film grain structures -I. Grain growth stagnation, Acta metall. mater. 38 (1990) 1455–1462, https://doi.org/10.1016/0956-7151(90)90114-V.
[29] D.J. Srolovitz, S.A. Safran, Capillary instabilities in thin films. I. Energetics, J. Appl. Phys. 60 (1986) 247–254, https://doi.org/10.1063/1.337689.
[30] J. Kudrman, J. Cadek, Relative grain boundary free energy and surface energy of some metals and alloys, Czechoslovak J. Phys. B 19 (1969) 1337–1342, https://doi.org/10.1007/BF01690833.
[31] K. Barmak, E. Eggeling, D. Kinderlehrer, R. Sharp, S. Ta'asan, A.D. Rollett, K.R. Coffey, Grain growth and the puzzle of its stagnation in thin films: the curious tale of a tail and an ear, Prog. Mater. Sci. 58 (2013) 987–1055, https://doi.org/10.1016/j.pmatsci.2013.03.004.
[32] P. Jacquet, R. Podor, J. Ravaux, J. Teisseire, I. Gozhyk, J. Jupille, R. Lazzari, Grain growth: the key to understand solid-state dewetting of silver thin films, Scripta Mater. 115 (2016) 128–132, https://doi.org/10.1016/j.scriptamat.2016.01.005.
[33] K. Barmak, J. Kim, C.S. Kim, W.E. Archibald, G.S. Rohrer, A.D. Rollett, D. Kinderlehrer, S. Ta'asan, H. Zhang, D.J. Srolovitz, Grain boundary energy and grain growth in Al films: comparison of experiments and simulations, Scripta Mater. 54 (2006) 1059–1063, https://doi.org/10.1016/j.scriptamat.2005.11.060.
[34] D. Chatain, D. Galy, Interfaces between Pb crystal and Cu surfaces, J. Mater. Sci. 41 (2006) 7769–7774, https://doi.org/10.1007/s10853-006-0551-4.
[35] C.M. Müller, R. Spolenak, Microstructure evolution during dewetting in thin Au films, Acta Mater. 58 (2010) 6035–6045, https://doi.org/10.1016/j.actamat.2010.07.021.
[36] C.V. Thompson, R. Carel, Stress and grain growth in thin films, Mech. Phys. Solids 44 (1996) 657473, https://doi.org/10.1016/0022-5096(96)00022-1.
[37] G.S. Rohrer, X. Liu, J. Liu, A. Darbal, M.N. Kelly, X. Chen, M.A. Berkson, N.T. Nuhfer, K.R. Coffey, K. Barmak, The grain boundary character distribution of highly twinned nanocrystalline thin film aluminum compared to bulk microcrystalline aluminum, J. Mater. Sci. 52 (9) (2017) 19–9833, https://doi.org/10.1007/s10853-017-1112-8.
[38] C.V. Thompson, Grain growth in thin films, Ann. Rev. Mater. Sci. 20 (1990) 245–268, https://doi.org/10.1146/annurev.ms.20.080190.001333.
[39] H. Komurasaki, T. Isono, T. Tsukamoto, T. Ogino, Evolution of step morphology on vicinal sapphire (1 1 0 2) surfaces accompanied with self-assembly of comb-shaped chemical domains, App. Surf. Sci. 258 (2012) 5666–5671, https://doi.org/10.1016/j.apsusc.2012.02.052.